



Impact of Taguchi Optimization in Fiber Surface Plasmon Resonance Sensors Based on Si₃N₄ Layer

N. Mudgal¹ · Kamal Kishor Choure¹ · Manoj Kumar Falaswal¹ · Rahul Pandey² · Ankit Agarwal² · Dinesh Bhatia³ · Ankur Saharia⁴ · Saurabh Sahu⁵ · G. Singh¹

Received: 28 September 2021 / Accepted: 9 March 2022 / Published online: 17 March 2022
© The Author(s) under exclusive licence to Sociedade Brasileira de Física 2022

Abstract

This article exhibits a fiber plasmonic sensor based on a silver (Ag) layer and a silicon nitride (Si₃N₄) layer with a wide dynamic range of refractive index sensing. The Taguchi (L9) orthogonal array method is applied to optimize the design parameters such as fiber core, sensing region length, and the thickness of Ag/Si₃N₄ layers. The performance of the structure is investigated for the full-width half maxima (FWHM) as the smaller the better (STB). The smaller FWHM favors accurate detection, high-quality factor, and better sensitive detection of biomolecules. With the use of analysis of variance (ANOVA), it is evident that for the normalized transmitted power, the Ag layer thickness contributes 47.36%, while the Si₃N₄ layer thickness contributes 0.06% only. Furthermore, the length of the sensing region has the highest dominating factor effect of 53.26% whereas the thickness of the Si₃N₄ layer has the least dominating factor effect of 6.90% on FWHM. This work has shown the highest sensitivity of 6287 nm/RIU whereas the quality factor and detection accuracy are 873.19 RIU⁻¹ and 87.31 respectively. Hence, Taguchi's optimization approach is suitable in multilevel optimization of different control factors that lead to the robust design of the fiber SPR sensor.

Keywords Taguchi optimization · Surface plasmon resonance · Silver · Silicon nitride · Sensor

1 Introduction

Surface plasmon resonance (SPR) is a well-known technique with potential sensing applications in a variety of domains, including biomedical science and environmental science [1, 2]. In recent years, the SPR sensor has gained popularity because of its label-free and real-time sensing [3, 4]. In traditional SPR sensing, a glass prism along with a thin metal film is employed to excite the surface plasmons (SPs) at the metal–dielectric interface. This phenomenon was first

described in 1968 by Kretschmann using a high refractive index (RI) prism to couple light at the metal–dielectric interface surrounded by the sensing medium, in which angular interrogation method was used to see the sharp dip in the reflectivity spectrum [5]. However, the bulky and movable prism setup limits the prism-based sensing approach. The growing expectation for miniaturized, low-cost sensors suitable for remote sensing has been attracting researchers to propose new fiber-based sensors. Lidberg et al. originally presented SPR technology in a fiber-based sensor in 1983, which initiated this technology in the SPR sensing applications. These types of sensors have been widely employed in biomedical science, food safety, biomolecules detection, and environmental protection, etc. [6–10]. In the fiber sensing approach, a glass prism is replaced with the fiber core that is used to guide light waves and a small portion of fiber cladding is removed. Over unclad fiber, a metal layer is produced. For the evaluation of sensor performance, the sample to be detected is positioned around the layer of metal, and the resonance wavelength shift with the RI change is observed [11, 12]. Silver, copper, and gold are the most common plasmonic active metals. These are produced on the

✉ N. Mudgal
mudgalnitesh@gmail.com

¹ Department of ECE, Malaviya National Institute of Technology, Jaipur, India

² Swami Keshvanand Institute of Technology, Management & Gramothan, Jaipur, India

³ University Departments, Rajasthan Technical University, Kota, India

⁴ Manipal University, Jaipur, India

⁵ Jabalpur Engineering College, Jabalpur, India

unclad fiber core's surface. In comparison to these materials, gold is extremely stable. Because silver and copper have weak chemical stability and these are supposed to oxidize fast. This makes them lesser stable for the SPR sensor. As a result, applying a protective layer on the surface of these layers is a feasible option for making an SPR sensor more durable [13–15]. In recent times, the use of transition metal dichalcogenide (TMDC) materials such as WSe₂, MoS₂, MoSe₂, and WS₂ is seen in SPR sensing. These materials serve as supporting materials for enhancing plasmons in SPR sensing [16–21].

In this work, a protective layer of silicon nitride (Si₃N₄) has been deposited over the surface of the Ag layer that makes this structure more stable. Si₃N₄ has a huge bandgap (~5 eV) and received interest due to its excellent chemical and thermal stability [22, 23]. Here, we have used the Taguchi method to optimize the designing parameters employed in the proposed fiber SPR sensor. In the traditional approach, one factor at a time is optimized such that when the thickness of one layer is optimized, the thickness of the other layer is kept fixed. This process makes the high numbers of optimization tests. Due to this reason, the parameters generated with this approach are not sufficient for the designing of such sensors. The Taguchi technique aids in the creation of a robust design by taking into account all of the sensor's control elements. As a result, a high-performance SPR biosensor can be made with a small number of tests.

2 Sensor Design Parameters

Taguchi's optimized design of the proposed fiber-based SPR sensor is represented in Fig. 1. Here, the fused silica fiber core having a diameter of 600 μm is utilized to carry light waves from one side of the fiber to another side, in which a 10-mm length of fiber cladding is removed. Fiber optic probe with 600 μm of core diameter can be fabricated by removing 10-mm cladding portion from the middle region of a fiber using a sharp blade. After that, acetone and de-ionized water can be used to clean the unclad area of the

fiber [24]. The RI of the fused silica core (n_{core}) may be calculated using the given dispersion equation [25]:

$$n_{\text{core}}(\lambda) = \left(1 + \frac{a_1 \lambda^2}{\lambda^2 - b_1^2} + \frac{a_2 \lambda^2}{\lambda^2 - b_2^2} + \frac{a_3 \lambda^2}{\lambda^2 - b_3^2} \right)^{1/2} \quad (1)$$

Here, $a_1 = 0.6961663$, $b_1 = 0.0684043$, $a_2 = 0.4079426$, $b_2 = 0.1162414$, $a_3 = 0.8974794$, and $b_3 = 9.896161$ are the Sellmeier coefficients and “ λ ” is the wavelength in nm [26]. Ag metal layer of the thickness of 50 nm is grown over the unclad portion of the fiber. Liquid-phase deposition technique can be used to deposit silver layer over the unclad surface of optical fiber [27]. The dielectric constant of this layer (ϵ_{Ag}) is computed using the given Drude relation [28]:

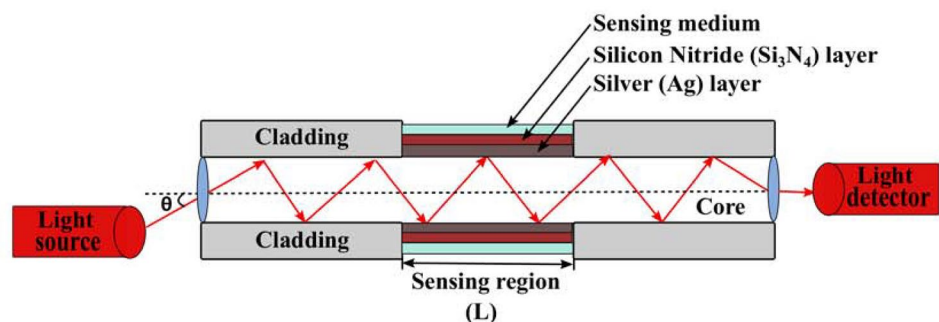
$$\epsilon_{\text{Ag}}(\lambda) = 1 - \frac{\lambda^2 \lambda_c}{\lambda_p^2 (\lambda_c + i\lambda)} \quad (2)$$

here, λ_c stands for collision (damping) wavelength and is defined as the wavelength corresponding to the damping of the oscillations of the electron density because of the collision among the electrons. The value of λ_c is 1.7614×10^{-5} m. Furthermore, λ_p stands for plasma wavelength. It is the wavelength that corresponds to the frequency of the electron density oscillations in the metal. The value of λ_p is 1.4541×10^{-7} m [29]. Next, to protect the silver layer from oxidation, a thin layer of Si₃N₄ of the thickness of 5 nm is grown over the covered region of the Ag layer. Magnetron sputtering technique can be used to deposit Si₃N₄ film on the surface of silver layer [30]. The dielectric constant for this can be computed using following relation [31]:

$$\epsilon_{\text{Si}_3\text{N}_4}(\lambda) = \left(1 + \frac{3.0249 \lambda^2}{\lambda^2 - 0.1353406^2} + \frac{40314 \lambda^2}{\lambda^2 - 1239.842^2} \right) \quad (3)$$

At the transmitting end of the fiber, light is incident and propagates through the fiber. The evanescent wave is generated at the metal surface that excites the SPs wave when the light wave is completely reflected in the detecting area. Lastly, we chose water as the detecting medium, which has a RI of 1.33 and measured the change in RI from 1.33 to 1.43

Fig. 1 Plasmonic fiber-based sensor structure



which is suitable for most of the biological reaction. We are restricted to this range because the resonance curve does not follow standardization after this range.

3 Mathematical Modeling

When p-polarized light is emitted into the transmitting end, it travels to the receiving end. In this, light propagates through the mechanism of total internal reflection (TIR). So the evanescent wave of the propagating ray can be used to excite the SPs [32]. The surface plasmon wave vector (β_{sp}) and incident light wave vector (k_x) should be identical for resonance. In terms of mathematics [33], the equation is as follows:

$$\beta_{sp} = k_x \tag{4}$$

$$\left\{ \frac{2\pi}{\lambda} \operatorname{Re} \sqrt{\frac{\epsilon_m \epsilon_{die}}{\epsilon_m + \epsilon_{die}}} \right\} = \frac{2\pi}{\lambda} n_{core} \sin \theta \tag{5}$$

where ϵ_m and ϵ_{die} signify the dielectric constant of metal and sensing medium respectively, n_{core} denotes the RI of the fiber core and λ denotes the incident light wavelength.

For p-polarized wave incident at transmitting end at angle θ , the normalized transmitted power (P_{trans}) at the receiving end of the fiber can be computed as follows [34] :

$$P_{trans} = \frac{\int_{\theta_{cr}}^{\pi/2} R_p^{N_{ref}(\theta)} \left(n_1^2 \sin \theta \cos \theta / (1 - n_1^2 \cos^2 \theta)^2 \right) d\theta}{\int_{\theta_{cr}}^{\pi/2} \left(n_1^2 \sin \theta \cos \theta / (1 - n_1^2 \cos^2 \theta)^2 \right) d\theta} \tag{6}$$

where $N_{ref} = L/D \tan \theta$ denotes the total number of reflections performed by the incident wave in the sensing region, D and L denote the core diameter and the sensing region length respectively, $\theta_{cr} = \sin^{-1} n_{cl}/n_{core}$ denotes the critical angle at the interface of the core-cladding while n_{cl} and n_{core} denote the RI of the cladding and core of the fiber respectively.

The Fresnel multilayer reflection theory is used to compute the reflectance (R_p) of this multilayer structure (core/metal/Si3N4/sensing medium) and is provided by [35].

$$R_p = r_p r_p^* = |r_p|^2 \tag{7}$$

For p-polarized light, the reflection coefficient (r_p) is as follows:

$$r_p = \frac{q_1 (M_{11} + M_{12}q_N) - (M_{21} + M_{22}q_N)}{q_1 (M_{11} + M_{12}q_N) + (M_{21} + M_{22}q_N)} \tag{8}$$

here, for the j^{th} layer, $M_j = \begin{bmatrix} \cos \beta_j & \frac{-i}{q_j} \sin \beta_j \\ -iq_j \sin \beta_j & \cos \beta_j \end{bmatrix}$ is the characteristic matrix, in which transverse RI $q_j = \sqrt{\left(\frac{1}{\epsilon_j}\right)}$ $\cos \theta_j = \sqrt{(\epsilon_j - n_1^2 \sin^2 \theta_1)}/\epsilon_j$ and phase factor $\beta_j = \left(\frac{2\pi}{\lambda}\right) n_j \cos \theta_j (z_j - z_{j-1})$; where $(z_j - z_{j-1})$ is the thickness of the j^{th} layer.

4 Sensor Performance Parameters

The sensor performance in this study is evaluated for sensitivity, quality factor, and detection accuracy. The sensitivity (S_λ) is expressed in terms of resonance wavelength change ($\delta\lambda$) and RI change (δn) and can be expressed as follows [36] :

$$S_\lambda = \frac{\delta\lambda}{\delta n} \left(\frac{nm}{RIU} \right) \tag{9}$$

The quality factor (Q) is determined by the ratio of sensitivity to FWHM and can be written as follows [37] :

$$Q = S_\lambda / FWHM (RIU^{-1}) \tag{10}$$

The FWHM of an SPR curve is the spectral width that corresponds to the 50% value of transmission spectra. The third important performance parameter is the detection accuracy which can be given by the ratio of $\delta\lambda$ to FWHM, mathematically [38] :

$$\text{Detection accuracy} = \delta\lambda / FWHM \tag{11}$$

5 Result Analysis and Discussion

The Taguchi technique is a popular tool for increasing efficiency in research and development. It uses a unique design of orthogonal arrays to examine control parameters with only the few trials, greatly reducing the number of tests and increasing efficiency. It aids in determining the impact of a variety of control elements on the device quality characteristics. Furthermore, signal to noise (SNR) ratio in the Taguchi technique aids researchers to quickly identifying the best combinations of the desired design specifications [39]. In the presented work, Taguchi L9 orthogonal array is used to optimize the different control parameters of this structure. The diameter of the fiber core, length of the sensing region, and the thickness of the silver layer and the silicon nitride layer are taken as control factors that mainly affect the performance of the designed

Table 1 Studied control factors and level representation

Control factors	Level 1	Level 2	Level 3
Core diameter (μm)	400	500	600
Length of sensing region (mm)	10	15	20
Thickness of silver layer (nm)	40	50	60
Thickness of Si_3N_4 layer (nm)	3	5	7

structure. These control factors are listed in Table 1. With these control factors, the appropriate orthogonal array is L9. FWHM and normalized transmitted power for all nine experiments can be calculated from Fig. 2. With the Taguchi array structure, the number of simulation trials has been cut from 81 (34) to 9 only. This saves cost, time, and the number of attempts while optimizing the SPR sensor's design parameters.

FWHM is the important parameter in designing of sensor that mainly gives the spectral width of the SPR curve. If the FWHM of the SPR curve is large, the quality factor and detection accuracy decrease as expressed in Eqs. 10 and 11 respectively. Here, we have optimized the performance for smaller the better SNR. Furthermore, SNR for the FWHM with the Si_3N_4 layer and without the Si_3N_4 layer is shown in Tables 2 and 3 respectively. It is seen that adding the Si_3N_4 layer reduces the FWHM which is the primary prerequisite for designing for such an SPR sensor. In Table 2, FWHM is calculated from the SPR curve that can plot with

the help of Fresnel multilayer reflection theory and transfer matrix method. Furthermore, Taguchi L9 orthogonal array is used to calculate SNR for the desired control factors that we can consider smaller the better for FWHM.

Mean and SNR are calculated for FWHM and normalized transmitted power for all nine experiments. In Taguchi design analysis, SNR can be categorized as larger the better, nominal the best, and smaller the best. In designing of fiber SPR sensor, small FWHM and large normalized transmitted power are the prerequisites. Normalized transmitted power with SNR (smaller the better) for different experiments is shown in Table 4. Here, SNR is selected for smaller the better for best performance of the proposed sensor that can be calculated by the following equation [40]:

$$\text{SNR}_{\text{Smaller the better}} = -10 \log_{10} \left(\frac{1}{n} \sum_{i=1}^n Y_i^2 \right) \quad (12)$$

here, n represents the number of trials and Y_i denotes the response for a specific factor-level combination.

5.1 Interpretation of Response Table for FWHM

The response table is utilized to determine the appropriate level for each control factor. Response characteristics of different control factors with SNR for FWHM are depicted in Table 5. In this, the factors with the greatest effect on FWHM are identified using rank values and delta. The rank

Fig. 2 SPR spectra of normalized transmitted power for different numbers of experiment

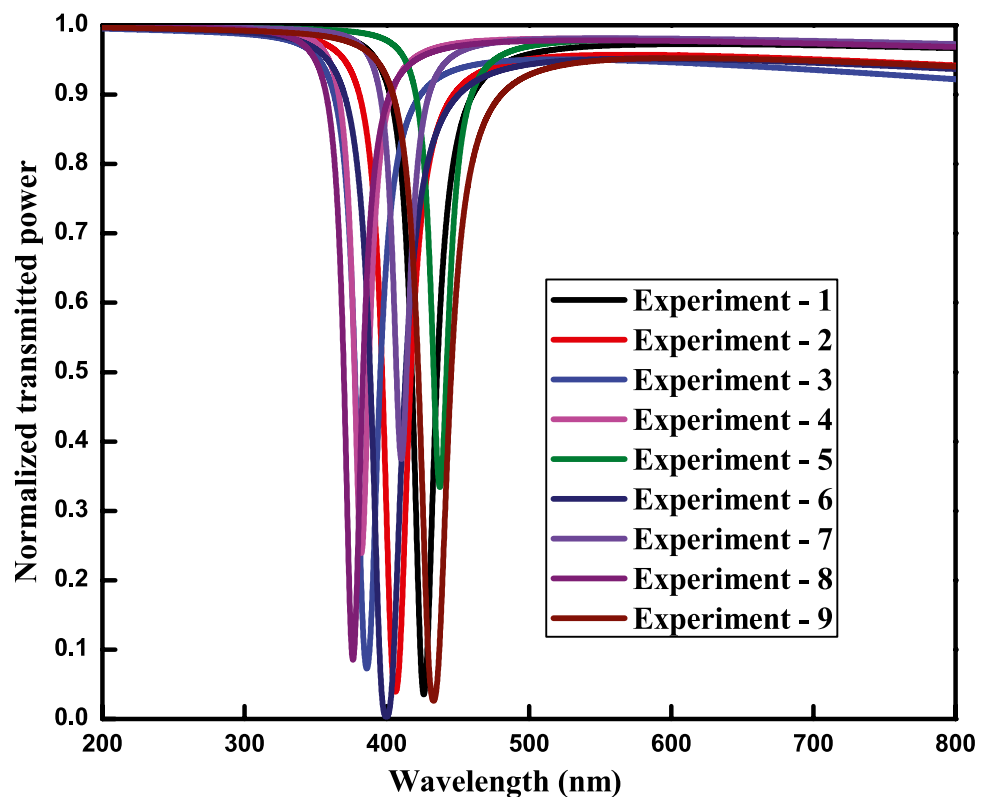


Table 2 FWHM with their SNR for different experiments

Experiment no.	Control factors				FWHM (nm)	SNR
	Core diameter (μm)	Length of sensing region (mm)	Thickness of silver layer (nm)	Thickness of Si ₃ N ₄ layer (nm)		
1	400	10	40	3	17.8	-25.0084
2	400	15	45	5	20.3	-26.1499
3	400	20	50	7	17.9	-25.0571
4	500	10	45	7	10.0	-20.0000
5	500	15	50	3	9.0	-19.0849
6	500	20	40	5	25.0	-27.9588
7	600	10	50	5	7.2	-17.1466
8	600	15	40	7	13.5	-22.6067
9	600	20	45	3	23.1	-27.2722

Table 3 FWHM with their SNR without the Si₃N₄ layer for different experiment

Experiment no.	Control factors			FWHM (nm)	SNR
	Core diameter (μm)	Length of sensing region (mm)	Thickness of silver layer (nm)		
1	400	10	40	21.2	-26.5267
2	400	15	45	27.6	-28.8182
3	400	20	50	28.5	-29.0969
4	500	10	45	16.8	-24.5062
5	500	15	50	11.7	-21.3637
6	500	20	40	33.5	-30.5009
7	600	10	50	12.4	-21.8684
8	600	15	40	21.2	-26.5267
9	600	20	45	27.6	-28.8182

Table 4 Normalized transmitted power with their SNR for different experiments

Experiment no.	Control factors				Normalized transmitted power	SNR (smaller the better) (STB)
	Core diameter (μm)	Length of sensing region (mm)	Thickness of silver layer (nm)	Thickness of Si ₃ N ₄ layer (nm)		
1	400	10	40	3	0.035250	29.0568
2	400	15	45	5	0.039170	28.1409
3	400	20	50	7	0.072900	22.7454
4	500	10	45	7	0.239200	12.4248
5	500	15	50	3	0.334400	9.5147
6	500	20	40	5	0.003253	49.7543
7	600	10	50	5	0.374600	8.5286
8	600	15	40	7	0.085310	21.3800
9	600	20	45	3	0.026070	31.6772

of sensing region length is one while the rank of silver layer thickness, core diameter, and Si₃N₄ layer is 2, 3, and 4 respectively. This means that the length of the sensing region has the highest contributing effect of smaller SNR for FWHM. The overall mean value of SNR for FWHM from Fig. 3 is obtained at -23.365.

5.2 Interpretation of Response Table for Normalized Transmitted Power

The response table for different control factors for the normalized transmitted power is shown in Table 6. In this, the thickness of the Ag layer with a delta value of 19.80 and

Table 5 Response table for SNR for different control factors for FWHM; smaller the better

Level	Core diameter (μm)	Length of sensing region (mm)	Thickness of silver layer (nm)	Thickness of Si_3N_4 layer (nm)
1	-25.41	-20.72	-25.19	-23.79
2	-22.35	-22.61	-24.47	-23.75
3	-22.34	-26.76	-20.43	-22.55
Delta	3.06	6.04	4.76	1.23
Rank	3	1	2	4

rank 1 has the highest factor in optimizing normalized transmitted power in designing the proposed SPR sensor. Furthermore, the length of the sensing region and thickness of the Si_3N_4 layer are having ranks 2 and 3 respectively. Here, the diameter of the fiber core had the lowest factor with rank 4 in optimizing the normalized transmitted power. The main effect plot of SNR representation for normalized transmitted power with different control factors is shown in Fig. 4. This plot indicates that the thickness of the silver layer has the highest factor effect on SNR for the normalized transmitted power.

5.3 Analysis of Variance (ANOVA) Interpretation

The analysis of variance (ANOVA), a popular statistical approach, is used to see which of the control factors had a significant impact on the performance parameters. ANOVA interpretation for FWHM and normalized transmitted power is given in Tables 7 and 8 respectively. The contribution of control factor was chosen to indicate the importance of a

Table 6 Response table for different control factors for normalized transmitted power; smaller the better

Level	Core diameter (μm)	Length of sensing region (mm)	Thickness of silver layer (nm)	Thickness of Si_3N_4 layer (nm)
1	26.65	16.67	33.40	23.42
2	23.90	19.68	24.08	28.81
3	20.53	34.73	13.60	18.85
Delta	6.12	18.06	19.80	9.96
Rank	4	2	1	3

control factor. The high percentage value of a contribution has the greatest impact on the FWHM and normalized transmitted power. From Table 7, it is clear that the length of the sensing region has the highest contribution factor effect of 53.27% on FWHM followed by thickness of the silver layer and core diameter with 29.83% and 10% respectively while the thickness of the Si_3N_4 layer has least contribution effect of 6.90% on optimization of the FWHM. ANOVA analysis for normalized transmitted power depicted in Table 8 shows that the thickness of the silver layer has the highest contribution factor effect of 47.36% on optimization of the normalized transmitted power followed by the length of sensing region and the core diameter with 31.58% and 21% respectively while the thickness of Si_3N_4 layer has the least contribution factor effect of 0.06% on optimization of the normalized transmitted power.

In conclusion, the best selection of control parameters with the Taguchi optimization method for designing the proposed SPR sensor is given in Table 9. Based on these

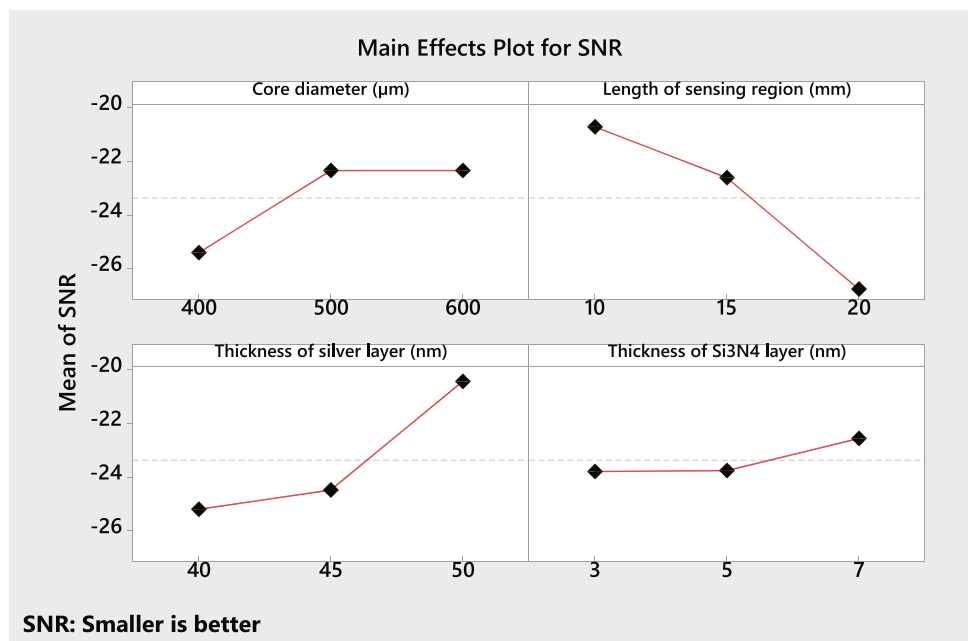
Fig. 3 SNR representation for FWHM with different control factors

Fig. 4 SNR representation for normalized transmitted power with different control factors

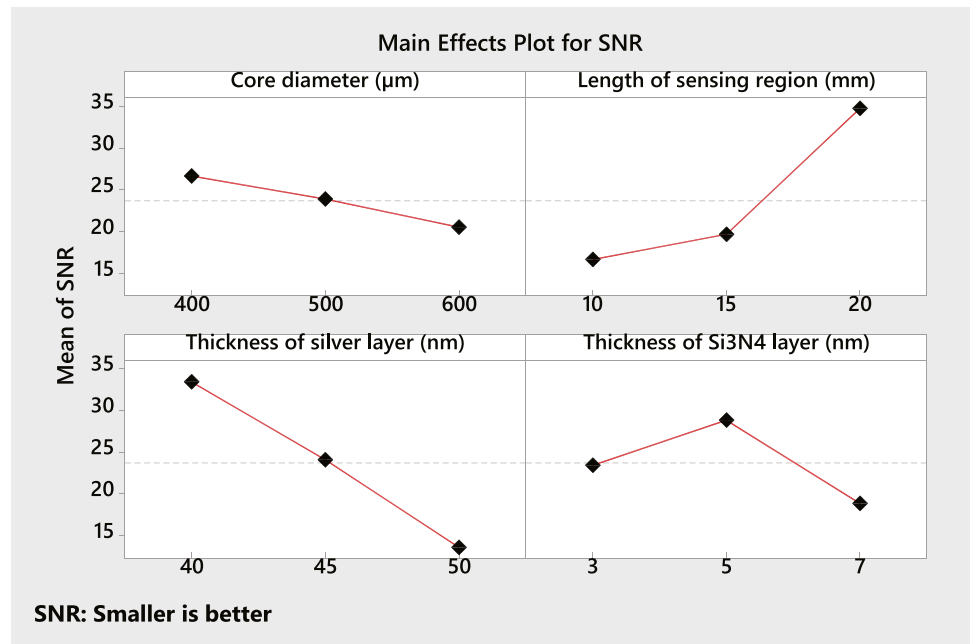


Table 7 Analysis of variance (ANOVA) for FWHM with different control factors

Control factors	Degree of freedom	Sum of square	Mean square	Contribution
Core diameter (μm)	2	32.54	16.27	10.00%
Length of sensing region (mm)	2	173.34	86.67	53.27%
Thickness of silver layer (nm)	2	97.08	48.54	29.83%
Thickness of Si_3N_4 layer (nm)	2	22.47	11.23	6.90%

Table 8 Analysis of variance (ANOVA) for normalized transmitted power with different control factors

Control factors	Degree of freedom	Sum of square	Mean square	Contribution
Core diameter (μm)	2	0.034161	0.017080	21.00%
Length of sensing region (mm)	2	0.051377	0.025688	31.58%
Thickness of silver layer (nm)	2	0.077075	0.038537	47.36%
Thickness of Si_3N_4 layer (nm)	2	0.000093	0.000047	0.06%

parameters, we have a designed a fiber SPR sensor for the RI ranging from 1.33 to 1.43. The plot for normalized transmitted power with RI of sensing medium is shown in Fig. 5a. In

this, when we are increasing the RI of the sensing medium, the resonance wavelength shifts to a higher value. The value of resonance wavelength for respective RI of sensing medium is plotted in Fig. 5b and also depicted in Table 10. The values of sensitivity, quality factor, and detection accuracy which are given in Table 10 can be calculated by using Eqs. 9, 10, and 11 respectively. Here, the maximum sensitivity of 6287 nm/RIU is achieved for the varying RI from 1.33 to 1.43 while the maximum quality factor and detection accuracy are 873.19 RIU⁻¹ and 87.31 respectively. As a result, the Taguchi approach can be utilized to optimize the designing parameters and can assist in designing the fiber SPR sensor.

Table 9 Best selection of control parameter with Taguchi method

S. no.	Control parameter	Parameter value
1	Core diameter (μm)	600
2	Length of sensing region (mm)	10
3	Thickness of silver layer (nm)	50
4	Thickness of Si_3N_4 layer (nm)	5

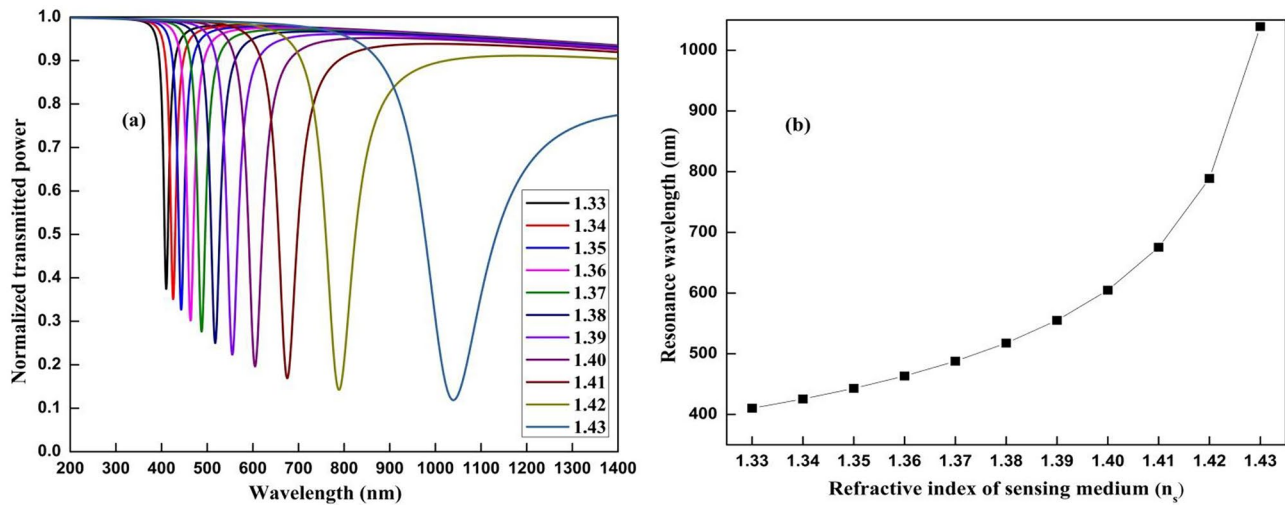


Fig. 5 (a) Plot of the SPR spectra and (b) the shift of resonance wavelength for the core-Ag-Si₃N₄ configuration with different RI of the sensing medium

Table 10 Performance characteristics of proposed structure for different RI of sensing medium

S. no.	RI of sensing medium	Resonance wavelength (nm)	Sensitivity (nm/RIU)	Quality factor (RIU ⁻¹)	Detection accuracy
1	1.33	410.3	-	-	-
2	1.34	425.5	1520	211.11	2.11
3	1.35	443	1635	227.08	4.54
4	1.36	463.4	1770	245.83	7.37
5	1.37	487.8	1937.5	269.09	10.76
6	1.38	517.6	2146	298.05	14.90
7	1.39	555.1	2413.33	335.18	20.11
8	1.40	604.8	2778.57	385.91	27.01
9	1.41	675.4	3313.75	460.24	36.81
10	1.42	788.8	4205.55	584.10	52.56
11	1.43	1039	6287	873.19	87.31

6 Conclusion

In a nutshell, this study focused on the use of numerical analysis, specifically transfer matrix method (TMM) and Taguchi's method, as an appropriate and reliable approach for improving the control parameters of a Si₃N₄-based fiber plasmonic sensor. Signal to noise ratio is kept smaller the better (STB) for both the FWHM and the normalized transmitted power. Using ANOVA analysis, firstly the thickness of the silver layer has the highest contribution of 47.36% while the thickness of Si₃N₄ has the least contribution of 0.06% for the normalized transmitted power. Secondly, on the FWHM, the length of the sensing region has the largest dominant factor effect of 53.26%, while the thickness of the Si₃N₄ layer has the least dominating factor effect of 6.90%. With Taguchi optimization, the best control

parameters which contribute maximum normalized transmitted power and minimum FWHM are 600 μ m of core diameter, 10 mm of the length of sensing region, 50 nm thickness of the silver layer, and 5 nm thickness of Si₃N₄ layer. Considering all these optimized parameters, the maximum sensitivity of 6287 nm/RIU is obtained while the quality factor and detection accuracy are 873.19 RIU⁻¹ and 87.31 respectively. Hence, the Taguchi optimization method is strongly suggested in nanotechnology due to its ability to optimize control factors in the endeavor to design effective fiber SPR sensors.

Acknowledgements The authors would like to express their gratitude to the Department of ECE at Malaviya National Institute of Technology, Jaipur, for providing critical support and facilities for this research work.

Declarations

Conflict of Interest The authors declare competing interests.

References

1. K.N. Shushama, M.M. Rana, R. Inum, M.B. Hossain, Graphene coated fiber optic surface plasmon resonance biosensor for the DNA hybridization detection: simulation analysis. *Opt. Commun.* **383**, 186–190 (2017)
2. M.S. Rahman, M.R. Hasan, K.A. Rikta, M.S. Anower, A novel graphene coated surface plasmon resonance biosensor with tungsten disulfide (WS₂) for sensing DNA hybridization. *Opt. Mater.* **75**, 567–573 (2018)
3. R. Zafar, S. Nawaz, G. Singh, A. d'Alessandro, M. Salim, Plasmonics based refractive index sensor for detection of hemoglobin concentration. *IEEE Sens. J.* **18**(11), 4372–4377 (2018)
4. Y. Saylan, S. Akgönüllü, D. Çimen, A. Derazshamshir, N. Bereli, F. Yilmaz, A. Denizli, Development of surface plasmon resonance sensors based on molecularly imprinted nanofilms for sensitive and selective detection of pesticides. *Sens. Actuators B Chem.* **24**, 446–454 (2017)
5. E. Kretschmann, H. Raether, Radiative decay of non-radiative surface plasmons excited by light. *Zeitschrift für Naturforschung A* **23**(12), 2135–2136 (1968)
6. N. Mudgal, P. Yupapin, J. Ali, G. Singh, BaTiO₃-graphene-affinity layer-based surface plasmon resonance (SPR) biosensor for pseudomonas bacterial detection. *Plasmonics* (2020)
7. A.A. Kolomenskii, P.D. Gerson, H.A. Schuessler, Sensitivity and detection limit of concentration and adsorption measurements by laser-induced surface plasmon resonance. *Appl. Opt.* **36**, 6539–6547 (1997)
8. L. Liu, M. Wang, L. Jiao, T. Wu, F. Xia, M. Liu, W. Kong, L. Dong, M. Yun, Sensitivity enhancement of a graphene–barium titanate-based surface plasmon resonance biosensor with an Ag–Au bimetallic structure in the visible region. *J. Opt. Soc. Am. B* **36**(4), 1108–1116 (2019)
9. N. Mudgal, M. K. Falaswal, T. Ismail, I. S. Fahim, M. Tiwari, G. Singh, *Study of approaches to implement the prism-based surface plasmon resonance sensors* ed. by. V. Janyani, G. Singh, M. Tiwari, T. Ismail. *Optical and Wireless Technologies (Lecture Notes in Electrical Engineering, 2020)* p. 648
10. A.S. Kushwaha, A. Kumar, R. Kumar, M. Srivastava, S.K. Srivastava, Zinc oxide, gold and graphene-based surface plasmon resonance (SPR) biosensor for detection of pseudomonas like bacteria: A comparative study. *Optik* **172**, 697–707 (2018)
11. A. Sharma, R. Jha, B.D. Gupta, Fiber-optic sensors based on surface plasmon resonance: a comprehensive review. *Sens. J. IEEE* **7**(8), 1118–1129 (2007)
12. Y. Zhao, R.J. Tong, X. Feng, P. Yun, Current status of optical fiber biosensor based on surface plasmon resonance. *Biosens. Bioelectron.* **142**, 111505 (2019)
13. S. Franzen, Surface plasmon polaritons and screened plasma absorption in indium tin oxide compared to silver and Gold. *J. Phys. Chem.* **112**(15), 6027–6032 (2008)
14. B. Liedberg, C. Nylander, M.I. Lunstro, Surface plasmon resonance for gas detection and biosensing. *Sens Actuators* **4**, 299–304 (1993)
15. L. Xia, S. Yin, H. Gao, Q. Deng, C. Du, Sensitivity enhancement for surface plasmon resonance imaging biosensor by utilizing gold-silver bimetallic film configuration. *Plasmonics* **6**(2), 245–250 (2011)
16. S. Zeng, D. Baillargeat, H.P. Ho, K.T. Yong, Nanomaterials enhanced surface plasmon resonance for biological and chemical sensing applications. *Chem. Soc. Rev.* **43**, 3426–3452 (2014)
17. A.K. Mishra, S.K. Mishra, R.K. Verma, Graphene and beyond graphene MoS₂: a new window in surface-plasmon-resonance-based fiber optic sensing. *J. Phys. Chem. C* **120**(5), 2893–2900 (2016)
18. J.B. Maurya, Y.K. Prajapati, V. Singh, J.P. Saini, R. Tripathi, Performance of graphene MoS₂ based surface plasmon resonance sensor using silicon layer. *Opt. Quant. Electron* **47**, 3599–3611 (2015)
19. Y. Luo, C. Chen, K. Xia, S. Peng, H. Guan, J. Tang, H. Lu, J. Yu, J. Zhang, Y. Xiao, Z. Chen, Tungsten disulfide (WS₂) based all-fiber-optic humidity sensor. *Opt. Express* **24**(8), 8956 (2016)
20. H. Shi, H. Pan, Y. W. Zhang, B.I. Yakobson, Quasiparticle band structures and optical properties of strained monolayer MoS₂ and WS₂. *Phys. Rev. B* **87**, 155304 (2013)
21. S. Kaushik, U.K. Tiwari, S.S. Pal, R.K. Sinha, Rapid detection of Escherichia coli using fiber optic surface plasmon resonance immunosensor based on biofunctionalized molybdenum disulfide (MoS₂) nanosheets. *Biosens Bioelectron* **126**, 501–509 (2019)
22. S.-L. Ku, C.-C. Lee, Optical and structural properties of silicon nitride thin films prepared by ion-assisted deposition. *Opt. Mater.* **32**, 956–960 (2010)
23. N. Mudgal, A. Saharia, K.K. Choure, A. Agarwal, G. Singh, Sensitivity enhancement with anti-reflection coating of silicon nitride (Si₃N₄) layer in silver-based surface plasmon resonance (SPR) sensor for sensing of DNA hybridization. *Appl. Phys. A* **126**(946), (2020)
24. V. Kapoor, N.K. Sharma, V. Sajal, Effect of zinc oxide overlayer on the sensitivity of fiber optic SPR sensor with indium tin oxide layer. *Optik* **185**, 464–468 (2019)
25. R.K. Verma, B.D. Gupta, Surface plasmon resonance based fiber optic sensor for the IR region using a conducting metal oxide film. *J. Opt. Soc. Am. A* **27**(4), 846–851 (2010)
26. C.Z. Tan, Determination of refractive index of silica glass for infrared wavelengths by IR spectroscopy. *J. Non-Cryst. Solids* **223**(1–2), 158–163 (1998)
27. X. Zhang, X. Zhu, Y. Shi, Fiber optic surface plasmon resonance sensor based on a silver-coated large-core suspended-core fiber. *Opt. Lett.* **44**, 4550–4553 (2019)
28. M.A. Ordal, L.L. Long, R.J. Bell, S.E. Bell, R.R. Bell, R.W. Alexander, C.A. Ward, “Optical properties of metals Al Co, Cu, Au, Fe, Pb, ni, Pd, pt, Ag, Ti, and w”, *Pure Appl. Opt. J. Eur. Opt. Soc. A* **11**, 1099–1119 (1983)
29. A.K. Sharma, G.J. Mohr, Theoretical understanding of an alternating dielectric multilayer-based fiber optic SPR sensor and its application to gas sensing. *New J. Phys.* **10**, 023039 (2008)
30. J. Kulczyk-Malecka, P.J. Kelly, G. West, G.C.B. Clarke, J.A. Ridealgh, Diffusion studies in magnetron sputter deposited silicon nitride films. *Surf. Coat. Technol.* **255**, 37–42 (2014)
31. K. Luke, Y. Okawachi, M.R.E. Lamont, A.L. Gaeta, M. Lipson, Broadband mid-infrared frequency comb generation in a Si₃N₄ microresonator. *Opt. Lett.* **40**, 4823–4326 (2015)
32. B.D. Gupta, S.K. Srivastava, R. Verma, Fiber optic sensors based on plasmonics, World Scientific Publishing. Chapter 4, 93–95 (2015)
33. N. Mudgal, A. Saharia, A. Agarwal, G. Singh, ZnO and Bi-metallic (Ag–Au) layers based surface plasmon resonance (SPR) biosensor with BaTiO₃ and graphene for biosensing applications. *IETE J. Res.* (2020). <https://doi.org/10.1080/03772063.2020.1844074>
34. X. Zhou, X. Li, T.L. Cheng, S. Li, G. An, Graphene enhanced optical fiber SPR sensor for liquid concentration measurement. *Opt. Fiber Technol.* **43**, 62–66 (2018)

35. N. Mudgal, A. Saharia, A. Agarwal, J. Ali, P. Yupapin, G. Singh, Modeling of highly sensitive surface plasmon resonance (SPR) sensor for urine glucose detection. *Opt. Quant. Electron.* **52**, 307 (2020)
36. L. Wu, J. Guo, Q. Wang, S. Lu, X. Dai, Y. Xiang, D. Fan, Sensitivity enhancement by using few-layer black phosphorus-graphene/TMDCs heterostructure in surface plasmon resonance biochemical sensor. *Sens. Actuat. B Chem.* **249**, 542–548 (2017)
37. Y. Saad, M. Selmi, M.H. Gazzah, A. Bajahzar, H. Belmabrouk, Performance enhancement of a copper-based optical fiber SPR sensor by the addition of an oxide layer. *Optik* **190**, 1–9 (2019)
38. A. Sharma, B.D. Gupta, Fiber optic sensor based on surface plasmon resonance with Ag–Au alloy nanoparticle films. *Photon. Nanostruct.-Fundam. Appl.* **3**, 30–37 (2005)
39. N.R. Mohamad, M.F.M.R. Wee, M.A. Mohamed, A.A. Hamzah, P.S. Menon, Multi-response optimization of chromium/gold-based nanofilm Kretschmann-based surface plasmon resonance glucose sensor using finite-difference time-domain and Taguchi method. *Nanomater. Nanotechnol.* (2020). <https://doi.org/10.1177/1847980420982119>
40. S. Sahu, J. Ali, P. Yupapin, G. Singh, Effectiveness of Taguchi method for the optimization of narrowband optical filters based on grating waveguides. *MicrosystTechnol* **25**, 789–795 (2019)

Publisher's Note Springer Nature remains neutral with regard to jurisdictional claims in published maps and institutional affiliations.